

Bubble structures and sonoluminescence in viscous liquids

Atiyeh Aghelmaleki^{1,3}, Sergey Lesnik², Hossein Afarideh³, Gunther Brenner², Robert Mettin^{1*}

¹*Third Institute of Physics, Georg-August-University Göttingen,
Friedrich-Hund-Platz 1, 37077 Göttingen, Germany*

²*Institute of Applied Mechanics, Clausthal University of Technology,
Adolph-Roemer-Straße 2A, 38678 Clausthal-Zellerfeld, Germany*

³*Department of Energy Engineering and Physics, AmirKabir University of Technology, Tehran 15875-4413, Iran*

*Email: Robert.Mettin@phys.uni-goettingen.de

Introduction

Intense ultrasonic fields in liquids lead to acoustic cavitation, i.e. nucleation, oscillation and motion of bubbles [1]. Under continued sonication, the bubbles can move and form structures [2], mainly due to acoustic (Bjerknes) forces. Furthermore, objects submerged in the liquid are attacked by collapsing bubbles, a phenomenon leading to the well-known ultrasonic cleaning, but also to surface erosion – the latter being one of the motivations of the present study. While most scientific investigations of acoustic cavitation are concerned with pure water, tap water or sea water, other liquids – different from water – have been less often in the focus. However, for a number of applications of intense ultrasound particularly liquids with higher viscosity are relevant. Examples can be found, for instance, in the food and chemical industries. Yet, the properties of acoustic cavitation and the bubble behavior in such more exotic media has been only sparsely documented in the past. From existing work, one can conclude that the type of liquid and its viscosity is indeed an important parameter, and acoustic cavitation in oils, acids, molten metals or ionic liquids cannot be simply extrapolated from the aqueous case. Here we report, as part of a larger systematic experimental study, on changes in bubble structures under an ultrasonic horn when viscosity is incrementally increased from the case of pure water. As well, sonoluminescence, i.e. the light emission of collapsing bubbles, is subject of investigation. The extremely bright sonoluminescence in sulfuric and phosphoric acid has raised interest in the details of bubble dynamics in viscous liquids, and several reports have already shown differences in these acids as compared to water [3,4,5]. Further results have been obtained in glycerine with the background of ultrasound application to metal melts and casting [6]. However, a good part of the observations in higher viscous liquids still lack a complete explanation, which motivates more fundamental studies. The applied background of our investigations is the support of metal dissolution in acids for recycling purposes by acoustic cavitation, see for instance [7].

Experimental section

The liquids were held in a cubic PMMA container of 6 cm edge length. They were sonicated from the top by an in house-built exponential titanium horn (sonotrode) with circular tip diameter of 1 cm, operating sinusoidally at 21 kHz, and submerged to 1 cm depth. The cavitating bubble oscillations and structures, and as well the peak-to-peak displacement of the horn tip as a function of applied voltage, were visualized with back illumination by a high-speed camera (Photron

APX-RS 250K) coupled to a long-distance microscope (K2, Infinity). Different patterns of bubble structures could be produced by variation of parameters such as viscosity, temperature, liquid height level, horn dipping, the amount of dissolved gas in the liquid, driving frequency and applied voltage (sonotrode displacement). In the following, all parameters were set fixed, except for viscosity and sonotrode displacement. Used liquids were 100% de-ionized (DI) water, and de-ionized aqueous solutions of 50% v/v, 80% v/v and 99.9% v/v ethylene glycol (EG). Viscosities at room temperature were 1, 2.8, 8 and 15.5 cP, respectively.

We explored different bubble patterns in each liquid for three categories of sonotrode displacement amplitude: low (2-5 μm), moderate (5-10 μm) and high (10-15 μm). Below the lower range of low amplitude regime (<2.5 μm), no cavitation was observed. A 2D color map of acoustic pressure field (Fig. 1) was experimentally obtained via hydrophone measurements in this case for water in a slightly different cuvette. It can be seen that there is a high pressure region right under the sonotrode tip that can be considered as a primary antinode. Moreover, a standing wave pattern with further high pressure regions (second and third antinode) in the middle and at the bottom are formed as a result of ultrasonic wave reflections from the walls.

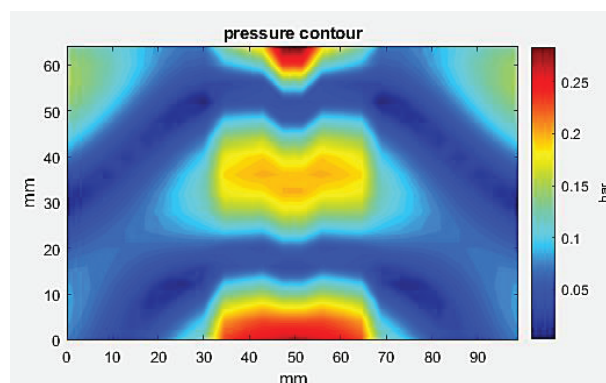


Figure 1: Measured sound pressure field in a similar cuvette for DI water at low amplitude. Pressure scale to the right.

Observations

An overview of changing bubble patterns with amplitude and viscosity is presented in Fig. 2 for the three categories of low, moderate and high pressure amplitude (top to bottom) in deionized water and aqueous solutions of 50%, 80% and 99.9% EG (left to right). The scale can be inferred from the 1 cm horn tip. The images show typical snapshots, although there exist certain dynamics in the bubble distributions, i.e., not in all cases a stationary pattern could be observed.

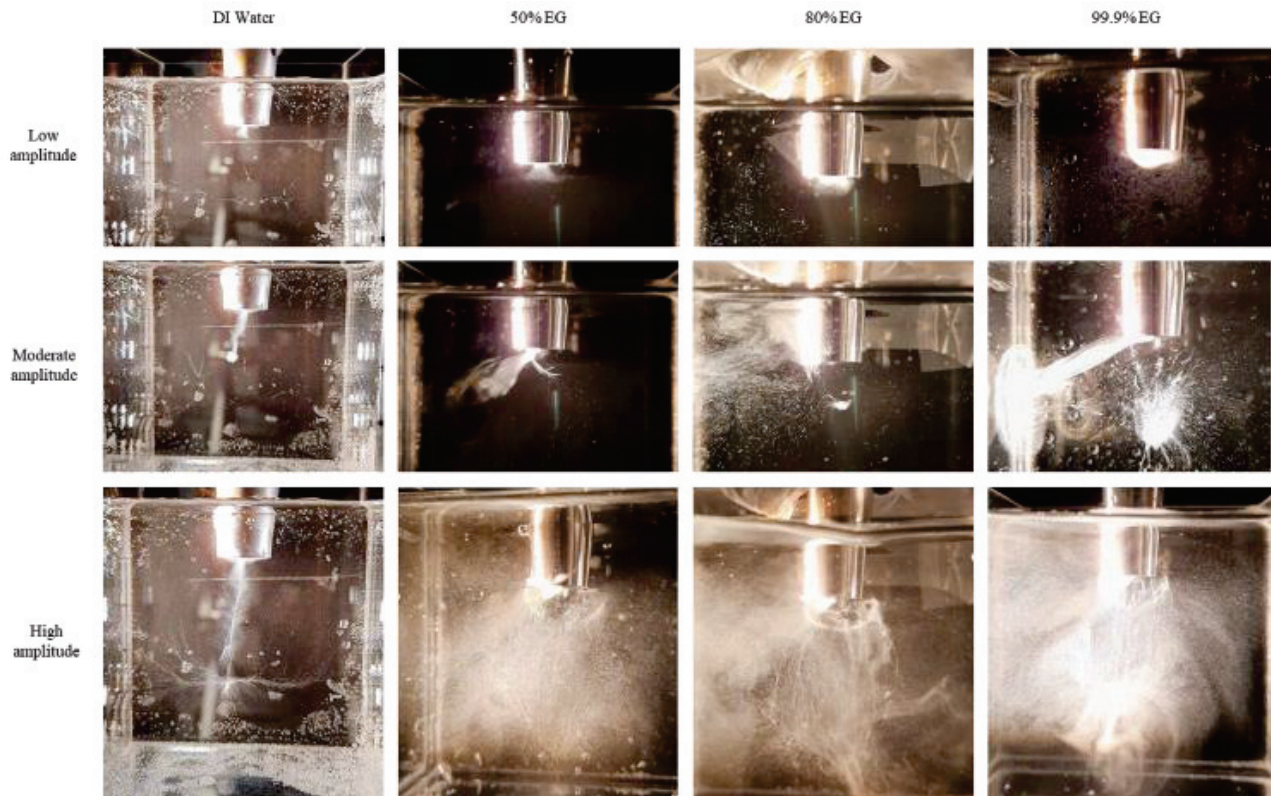


Figure 2: Typical images of bubble distribution for the varying viscosities (from left to right) and amplitudes (top to bottom).

Deionized water (DI)

The first column of Fig. 2 shows pure DI water as a reference. In the low amplitude regime, a short cylindrical bubble jet appears in which roughly three types of bubbles with different sizes and behavior occur (Fig. 3): (i) A large bubble is attached to the tip, oscillating between about 100 to 500 μm in diameter. It undergoes surface distortions and instabilities, splitting off many small bubbles during collapse. (ii) These split-off bubbles are quite small with diameters from a few micrometers to sub-micrometers (bubbly “mist”). They slowly move several millimeters downward, away from the sonotrode tip. Some of these small bubbles in the middle of their way grow larger due to collisions and/or rectified diffusion and form the larger bubbles of the next category. (iii) These medium-sized bubbles show large oscillations with a diameter variation in the range of 5-50 μm . They move again up towards the large bubble and sonotrode tip with speeds much faster than the small bubbles. The medium-sized bubbles can jump several 100 micrometers in an acoustic cycle and often are observed to undergo jetting in their collapse phase. All these three types of bubbles oscillate and collapse with the acoustic pressure field, although their maximum expansions are not completely in phase with each other due to the different sizes. This type of bubble population has been characterized before and is well-known [8,9,10], although it is not fully understood yet. The inversion of motion (up instead of down) with growing bubble (equilibrium) size is probably due to an increase in upward pointing primary Bjerknes force. Thus, the force due to liquid streaming, which is directed mainly downwards and carries the small bubbles, can be overcome once the bubble is beyond

the Blake threshold and is oscillating stronger. Jetting is mainly induced by the fast translation [8].



Figure 3: Large, medium and small bubbles for low amplitude pressure field. The gray horizon on the top is the sonotrode tip surface. Time difference between each image is 66.6 μs , and the frame width is 1.13 mm.

When increasing the applied voltage, the length of the bubble jet increases, but the behavior of large, medium and small bubbles in the structure is similar to lower amplitude. However, in a region a few centimeters below the sonotrode where the second antinode exists, some streamer-structures of bubbles form. These streamers join together and migrate inwards to a center where they accumulate and form a larger cluster (‘Acoustic Lichtenberg Figure’) [1,2]. A few numbers of Lichtenberg structures are gathered on the surface of an empty region which is probably containing the repulsive antinode. This repulsive antinode region expands with further increase of the applied voltage. Also, the bubble jet structure becomes longer and is affected by the repulsive force. Dendritic streamers now join the bubble jet body from the side, and the free tip of bubble jet deforms to a “flower” shape due to the repulsion. In the high amplitude regime, the bubble jet grows even longer and reaches the center of the second antinode region. When this happens, all streamers around reach the tip of the bubble jet and construct an upside-down

“tree” shape. Possibly the higher bubble density leads to a drop of the antinode pressure.

Viscous solutions of Ethylene Glycol

It gets obvious from the images in Fig. 2 that viscosity plays a significant role for the formed bubble structures. Even the smallest variation investigated, i.e., an increase from 1 cP (DI water) to 2.8 cP in the case of 50% EG, caused considerable changes of bubble patterns. As for the low amplitude regime, it can be seen that the short cylindrical bubble jet in the case of DI water deforms to a broad mushroom-like jet in which the presence of three types of large, medium and small bubbles is still recognizable. A large bubble remains attached to the bottom surface of the sonotrode like in the DI water case. Medium bubbles are in the middle, and small bubbles move down further to the broad edge of the mushroom, and then turn back towards the tip. Again, expansion and collapse of the different sizes of bubbles are not in phase with each other. The edges of this mushroom structure tend to bend outwards and upwards towards the sonotrode tip with increasing viscosity. In addition one can observe that other bubbles in the liquid far from the mushroom jet are attracted by the horn tip. Fig 4 shows the broad mushroom structure at lower amplitude for 99.9% EG. The edges of mushroom almost attached to the sonotrode surface in the case of 99.9% EG. Moreover, it seems that the number of visible bubbles at fixed pressure amplitude increases with viscosity.



Figure 4: Evolution of the mushroom structure in the case of 99.9% EG at low amplitude. Time difference between each image is 0.37 μ s, frame width 10.1 mm. Sonotrode tip surface on the top.

When it comes to moderate amplitudes, the mushroom jet transitions via a quick vortex transformation to an oblique bubble jet which is almost perpendicular to the sonotrode. Moreover, a bow structure (sickle-shape) beneath the sonotrode surface appears. Bubbles below it absorb to this bow structure, while there appears an empty space with no bubbles between the tip and the bow (Fig 5).



Figure 5: Side jet and bow structure.

The head of the bow is attached to and originates from the oblique bubble jet, whereas the tail of the bow is positioned freely under empty region. The presence of a bow structure diminishes with higher viscosities, and bubbles tend to accumulate in an interesting cloud or cluster-like structure.

The higher the viscosity, the more such cloud structures are observed, sometimes accompanied by a bow structure.

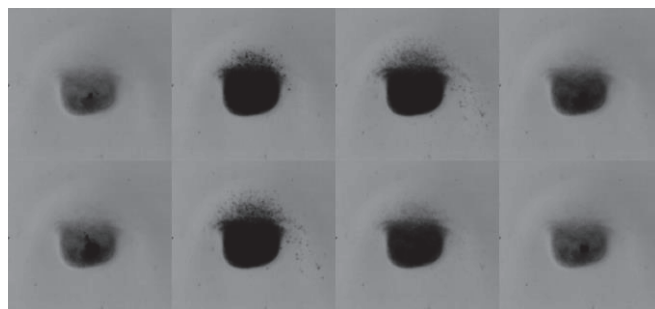


Figure 6: Bubble cloud structure for 99.9% EG. Time difference between each image is 0.37 μ s, and the frame width is 6.86 mm.

Fig. 6 shows a bubble cloud structure for 99.9% EG. This cloud, here below the center of the cuvette, consists mostly of small bubbles, with one or more large bubbles inside the cloud. The lower part of this bubble ensemble forms a surprisingly sharp boundary, while the upper part is more open and contains streamers. The small bubbles in the cloud appear to keep their distances somehow and move as a whole together. The large bubble inside the cloud undergoes rather intense collapses and seems to determine the movement of the cloud. Also, the oscillation of large and small bubbles of the cloud has some shift in phase. The cloud can both absorb other neighbor bubbles from the liquid and shoot some medium bubbles out into the liquid. Further, it can merge with other clouds. When the structure moves, it leaves tracks in form of small bubbles behind, probably split off from the larger oscillating bubble because of surface instabilities.

Further increasing the applied voltage leads to a particular hemispherical structure that appears like an “extended” bow structure, i.e., there are no bubbles inside the hemisphere, but rather on the surface of it. This peculiar hemispherical pattern was seen in all viscous solution of 50%, 80% and 99.9% EG in the high amplitude regime. The structure has been observed before in sulfuric acid experiments that focused on obtaining bright sonoluminescence light [11,3,4,5]. Also, in this regime the oblique bubble jet and an attraction zone can exist where bubbles seem to reach to a point below the hemisphere, in the shape of streamers. Such a structure is shown in Fig. 7 for 80% EG solution.

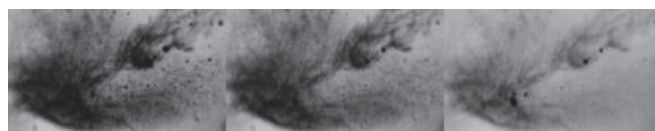


Figure 7: Bubble structure at attraction zone. Time difference between each image is 0.37 μ s, and the frame width is 10.9 mm.

Discussion

It seems that at low amplitude regime, the high pressure area below the sonotrode tip (the primary antinode) has an attraction force upon bubbles. However, with increasing the driving amplitude, the attractive antinode converts to a strong repulsive antinode, which makes bubbles move away from the sonotrode towards a surface. This transition shows itself via formation of a vortex that instantly repulses bubbles from the area by an oblique bubble jet which is accompanied by a bow-cloud/hemisphere structure. Since the force is still attractive

in the outer regions of the standing wave, a stable equilibrium surface forms around the antinode which is the bow and hemisphere surface structure. The equilibrium surface consists of some stationary bubbles, with certain range of size (Fig. 8) that can stay and oscillate on it. This can be due to the primary and secondary Bjerknes forces acting on and between the bubbles, keeping them together. The behavior is reminiscent to the equilibrium surfaces observed in few-bubble systems in a standing acoustic wave in sulfuric acid [12]. It seems that the repulsive antinode is also responsible for the oblique behavior of bubble jet. As for the attraction zone, we see small and large bubbles attract to this area from above or sides. These bubbles migrate inwards to a center – in the form of streamers – where they accumulate and form a larger cloud. Similar structures have been reported in sulfuric acid as well [5].

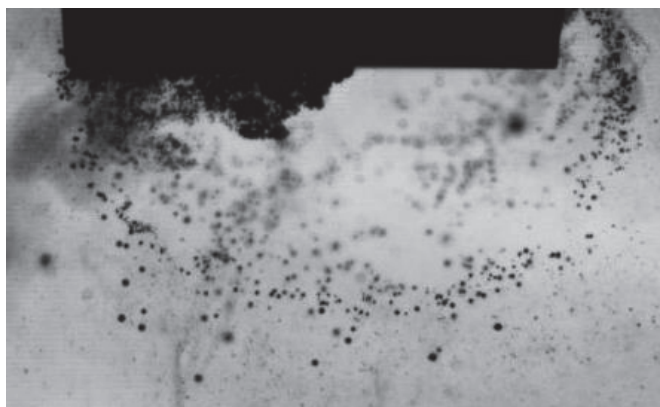


Figure 8: Hemispherical bubble structure at the horn tip (80% EG).

The difference of bubble patterns as compared to pure water is still to be clarified. Antinode repulsion by primary Bjerknes forces at high amplitude [13] should not be too sensitive to viscosity, but significant influence is expected on the drag forces counteracting bubble translation. Thus bubble motion should slow down. Generic acoustic streaming does not scale with viscosity, although it does not occur without dissipation (viscosity enters both in the driving force and in the drag force, and it cancels out [14]). Here, however, it appears as if the mushroom structure is based on a reduced penetration depth of streaming vortices due to the higher viscosity. This might be explained by the modified dissipation and driving of streaming in the presence of bubbles [9], but has to be explored further. Also the lifetime of individual bubbles appears to be extended in higher viscous liquid, although we cannot present a statistics here. Reasons might be higher damping of surface mode oscillations leading to higher shape stability, but as well aspects influencing gas diffusion and bubble dissolution, e.g. lower surface tension and lower diffusion coefficients. Still another aspect is the possible need for a modification of the force balance on the bubbles, since Basset (history) forces can come into effect at higher viscosity [15].

With respect to sonoluminescence, observed emissions have been quite weak and were mainly concentrated near the sonotrode tip. This remains in contrast to the very bright emission in sulfuric or phosphoric acid. Further studies with dissolved noble gases are planned to better explore the role of viscosity for the extremely bright flashes from some acids.

Conclusion

We have presented preliminary results of a larger study on acoustic cavitation bubble dynamics and structures in liquids of viscosity higher than water. Here, a sonotrode setup at 21 kHz was studied. In all liquids investigated, visible bubble numbers seem to grow with viscosity (at fixed driving amplitude), and bubble patterns change in comparison to pure water. As a peculiar feature, we observe a hemispherical structure under the sonotrode tip reported before for acids. This leads to the conclusion that viscosity is a major parameter in acoustic cavitation, and that some universal features of bubble structures in higher viscous liquids can be expected irrespective of the exact nature of the liquid.

Acknowledgements

We thank the mechanical and electrical workshops at Third Institute of Physics. Many thanks go also to Dwayne Stephens and Julian Eisener for help with the automatic pressure measurements. Support by the German Research Foundation (DFG) under the projects ME 1645/5-2 and BR 1864/12-2 is gratefully acknowledged.

References

- [1] Lauterborn, W., Kurz, T.: Physics of bubble oscillations. Rep. Prog. Phys. 73 (2010), 106501.
- [2] Mettin, R.: Bubble structures in acoustic cavitation In: A. A. Doinikov (ed.): Bubble and Particle Dynamics in Acoustic Fields: Modern Trends and Applications, Research Signpost, Kerala, India (2005), pp. 1-36.
- [3] Xu, H., Eddingsaas, N.C., Suslick, K.S.: Spatial separation of cavitating bubble populations: the nanodroplet injection model. J. Am. Chem. Soc. 131 (2009), 6060.
- [4] S. Hatanaka: Sonoluminescence of alkali-metal atoms in sulfuric acid: comparison between ultrasonic horn and cleaner. Proc. Symp. Ultrason. Electron. 31 (2010), 431–432.
- [5] Thiemann, A., Holsteys, F., Cairós, C., Mettin, R.: Sonoluminescence and dynamics of cavitation bubble populations in sulfuric acid. Ultrason. Sonochem. 34 (2017), 663.
- [6] Tzanakis, I., Lebon, G.S.B., Eskin, D.G., Pericleous, K.A.: Characterizing the cavitation development and acoustic spectrum in various liquids. Ultrason. Sonochem. 34 (2017), 651.
- [7] Pesic, B., Zhou, T.: Application of ultrasound in extractive metallurgy: Sonochemical extraction of nickel. Metall Mater Trans B 23 (1992), 13–22.
- [8] T. Nowak, R. Mettin: Unsteady translation and repetitive jetting of acoustic cavitation bubbles. Phys. Rev. E 90 (2014), 033016.
- [9] T. Nowak, C. Cairós, E. Batyrshin, R. Mettin: Acoustic streaming and bubble translation at a cavitating ultrasonic horn. AIP Conf. Proc. 1685 (2015), 020002-1 – 9.
- [10] Yasui, K., Iida, Y., Tuziuti, T., Kozuka, T., Towata, A.: Strongly interacting bubbles under an ultrasonic horn. Phys. Rev. E 77 (2008), 016609.
- [11] T. Lepoint, personal communication (2004)
- [12] Rosselló, J.M., Dellavale, D., Bonetto, F.J.: Stable tridimensional bubble clusters in multi-bubble sonoluminescence (MBSL). Ultrason. Sonochem. 22 (2015), 59-69.
- [13] Mettin, R., Luther, S., Ohl, C.D., Lauterborn, W.: Acoustic cavitation structures and simulations by a particle model. Ultrason. Sonochem. 6 (1999), 25.
- [14] Nyborg WL.: Acoustic streaming due to attenuated plane waves. J. Acoust. Soc. Am. 25 (1953), 68-75.
- [15] Magnaudet, J., Legendre, D.: The viscous drag force on a spherical bubble with a time-dependent radius. Phys. Fluids 10 (1998), 550.